THE JOURNAL OF PHYSICAL CHEMISTRY B

ARTICLE

pubs.acs.org/JPCB

Effect of Polyelectrolyte Architecture and Size on Macroion−Dye Assemblies

Immanuel Willerich, Torben Schindler, and Franziska Gröhn*

Department of Chemistry and Pharmacy and Interdisciplinary Center for Molecular Materials, Friedrich-Alexander University Erlangen-Nürnberg, Egerlandstrasse 3, 91058 Erlangen, Germany

Supporting Information

ABSTRACT: This study describes the influence of polyelectrolyte building block nature on the formation of supramolecular polyelectrolyte−dye nanoparticles self-assembled through electrostatic interactions of the oppositely charged building units and $\pi-\pi$ interactions in-between dye molecules ("electrostatic self-assembly"). The anionic azo dye Acid Red 26 (Ar26) is combined with cationic polyamidoamine dendrimers of generations G0, G2, G4, G6, and G8 and linear polycations polylysine (PolyLys) and polyallylamine hydrochloride (PAH). Light scattering reveals defined supramolecular particles with hydrodynamic radii R_H = 15 nm to R_H = 50 nm for slight excess of G2−G8 dendrimers. G0 does not yield stable assemblies. Linear polyelectrolytes form assemblies with hydrodynamic radii from R_H = 20 nm to R_H = 200 nm. Thermodynamic measurements by isothermal titration calorimetry (ITC) show that all macroions bind dye molecules up to about charge stoichiometry, and assembly formation is predominantly enthalpically driven. Differences in dye−dye interactions are related to structural features by analyzing endothermic heats of aggregate disruption through excess macroion addition. A simple model connects thermodynamic parameters with the internal assembly structure.

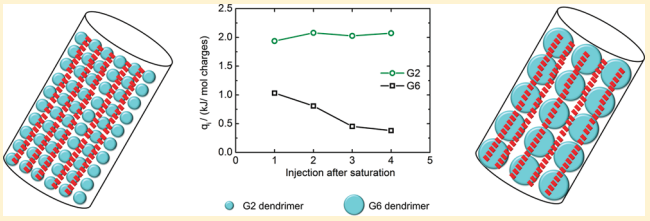

INTRODUCTION

Polymers and especially polyelectrolytes are useful building blocks for self-assembly into various composite structures.[1−10] When combined with oppositely charged surfactants,[11−17] metal counterions,[18−20] or other polyelectrolytes,[21−25] solid composite materials, organic−inorganic hybrid particles, or capsules can evolve.[26−30] A versatile class of current interest nanostructures are polyelectrolyte−dye associates, which are promising for optical materials or in wastewater treatment.[31−34] Moreover, porphyrin−polypeptide interactions are crucial in biologic processes, such as for example photosynthesis.[35] Therefore, studying polyelectrolyte−dye structures is of interest from a fundamental and practical point of view. Most previous studies have however focused either on solid-state structures or on the cooperative binding process of particular dyes to polyelectrolytes by spectroscopy, but not on the nanoscale particle formation.[36−43] While few studies on solution assemblies of polyelectrolytes and oppositely charged surfactants exist,[15−17,44,45] the field of polyelectrolyte−dye assemblies in solution hence is a promising road to new supramolecular nanoparticles. Recently, we introduced "electrostatic self-assembly" as a concept where well-defined nanoparticles are created in aqueous solution by self-assembly of polyelectrolytes and oppositely charged multivalent dye counterions.[46−56] Nanosize assemblies instead of mere host−guest structures are formed as the counterions interconnect the polyelectrolyte building blocks into structures incorporating multiple polyelectrolyte molecules resulting in particle sizes of 20−100 nm. Driving forces for the self-assembly process are electrostatic interactions between the oppositely charged building blocks and $\pi-\pi$ stacking in-between the dye counterions, while assemblies are afterward stabilized in solution through their excess charge.[50] This recent method toward nanoparticles is especially interesting as nanoparticles in solution can be formed by simple mixing because both building blocks are soluble in water, being a widely available and environmentally safe solvent, and because no sophisticated binding motif has to be created synthetically. In addition, the size of the assemblies can be triggered by external stimuli like pH and light irradiation, yielding promising responsive systems.[46,51,56] These properties may hence enable the concept to be useful for applications in sensors, coatings, or delivery systems.

In previous studies, we investigated a model system consisting of a cationic fourth-generation polyamidoamine dendrimer and a set of anionic aromatic azo dyes.[46,47,50,51] There, we demonstrated pH and light switchability[46,51] and studied size, shape, stability, and driving forces in dependence on the dye counterion.[47,50] Also, kinetic versus thermodynamic effects have been discussed.[50] In different systems, it was shown that the concept is applicable also to different polyelectrolyte architectures and counterions of different chemistry, e.g., using DNA,[48] cylindrical polymer brushes,[52,54,57,58] and linear polyelectrolytes[53,54] as the macroion component and, for example, extending the concept to porphyrin counterions.[52,54,57,58] While this variety demonstrated the overall versatility of the concept, detailed fundamental insight is expected when varying the polyelectrolyte

Received: May 10, 2011
Revised: July 6, 2011
Published: July 22, 2011

Scheme 1. Building Blocks Used for Electrostatic Self-Assembly in This Study[a]

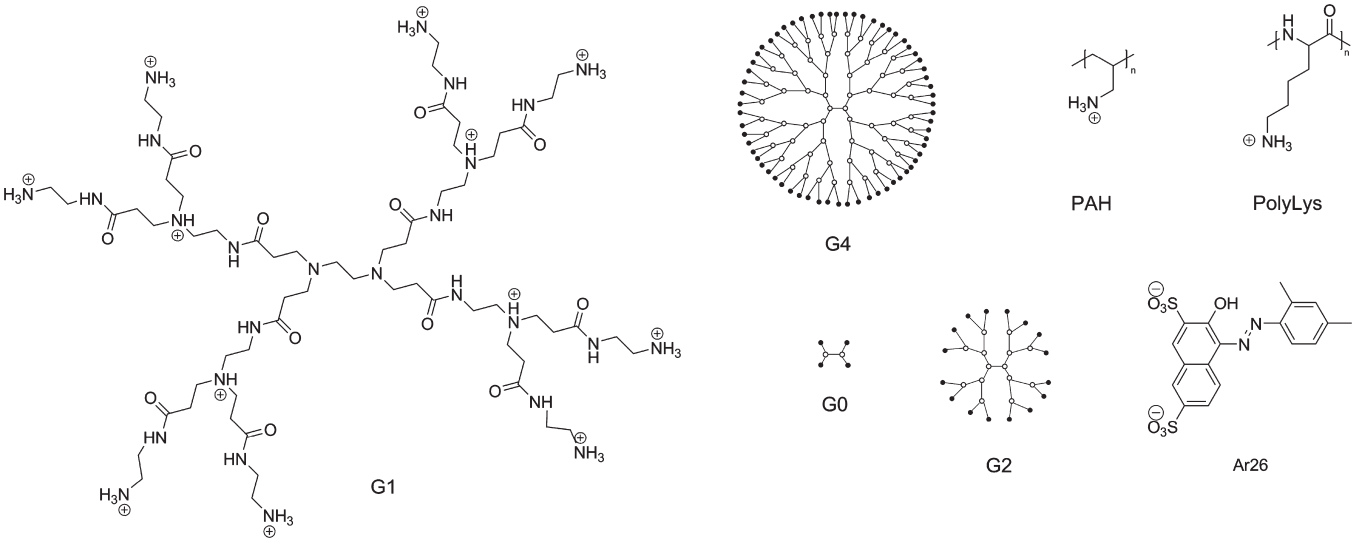

[a] G6 and G8 dendrimers were also used. The G1 molecular structure was depicted for added clarity only.

architecture using the same dye as a model counterion and analyzing the physical chemistry of structure formation, i.e., the size—thermodynamics relation, in detail.

Herein, it is hence now of interest whether the azo-dye macroion system can be extended to linear polyelectrolytes and to investigate fundamentally how polyelectrolyte size and architecture influence the assembly formation. This can on the one hand potentially extend a more specialized dendrimer-based model system to versatile systems of widely available linear polyelectrolytes and on the other hand yield fundamental insight into the role of the macroion in the structure direction.

In this study, therefore, different generations of cationic polyamidoamine (PAMAM) dendrimers as well as the linear polycations polylysine and polyallylamine are combined with the anionic azo dye Acid Red 26 (Ar26) as one selected model counterion. Building blocks are depicted in Scheme 1. The macroion component covers a size range from 1.5 to 10 nm,[59] i.e., from a typical low molecular mass molecule to a typical "polymer". Of main interest are assembly sizes, stoichiometries, and thermodynamics.

EXPERIMENTAL SECTION

Chemicals. Polyallylamine hydrochloride (PAH; molecular mass M_w = 17 000 g mol^{-1}) and polylysine hydrochloride (PolyLys; molecular mass M_w = 11 400 g mol^{-1}) were purchased from Aldrich. Polyamidoamine dendrimers of generations 0, 2, 4, 6, and 8 were obtained from Dendritech, Midland, MI, USA. Radius and size distribution given by the supplier were confirmed by DLS and HPLC (see Supporting Information). Acid Red 26 was obtained from Acros, Geel, Belgium, and purified to >98 wt % content by multiple recrystallizations from water and ethanol.[47,50]

Sample Preparation. Stock solutions were prepared in Milli-Q ultrapure water (>18.2 MΩ cm^{-1}) at the desired pH where the polyelectrolyte building blocks are fully deprotonated (either pH = 10.5 or pH = 11.5, see below). pH values were adjusted by adding the calculated amount of NaOH or HCl standard solutions. All pH values were counter-checked with a freshly calibrated pH electrode. The standard concentration of charged monomers in this study was c (charges) = 3.5 × 10^{-4} mol L^{-1} for light-scattering measurements. This corresponds to mass concentrations of c = 0.04 g L^{-1} for the dendrimers.

Preparation Method. An aqueous solution of the dye at pH = 10.5 (pH = 11.5 for PAH and PolyLys) was diluted with Milli-Q ultrapure water adjusted to pH = 10.5 (pH = 11.5 for PAH and PolyLys). Polymer stock solution at the same pH was added. After mixing, the appropriate amount of HCl was added at once under turbulent mixing to adjust the sample to pH = 3.5 inducing assembly formation.

Light Scattering. Measurements were carried out using an ALV CGS 3 goniometer and an ALV 5000 correlator with 320 channels (ALV Langen, Germany). A HeNe laser with a wavelength of λ = 632.8 nm with 22 mW output power was used. Measurements covered a range of scattering angles of 30° ≤ θ ≤ 150°. For each angle, the intensity autocorrelation function $g^2(\tau)$ was transferred into the electric field autocorrelation function $g^1(\tau)$ via the Siegert relation, and the latter transformed into the distribution of relaxation times by a regularized inverse Laplace transformation using the CONTIN algorithm developed by Provencher.[60] Mean relaxation times were then transferred into apparent diffusion coefficients $D_{app}(q)$. $D_{app}(q)$ was extrapolated to zero scattering vector q^2, and the extrapolated values yielded the hydrodynamic radii through the Stokes—Einstein formula

$$D_{app}(q^2 = 0) = \frac{kT}{6\pi\eta R_H} \quad (1)$$

where kT is the thermal energy and η the solvent viscosity. The widths of the size distributions are given by the standard deviation σ of the intensity weighted relaxation time distribution with logarithmic τ-axis.

Radii of gyration were calculated from static light-scattering data according to the Zimm equation

$$\frac{Kc}{R(\theta)} = \frac{1}{M_w}\left(1 + \frac{1}{3}q^2 < R_G^2 >\right) + 2A_2c \quad (2)$$

M_w is the weight average of the molecular mass, K the optical

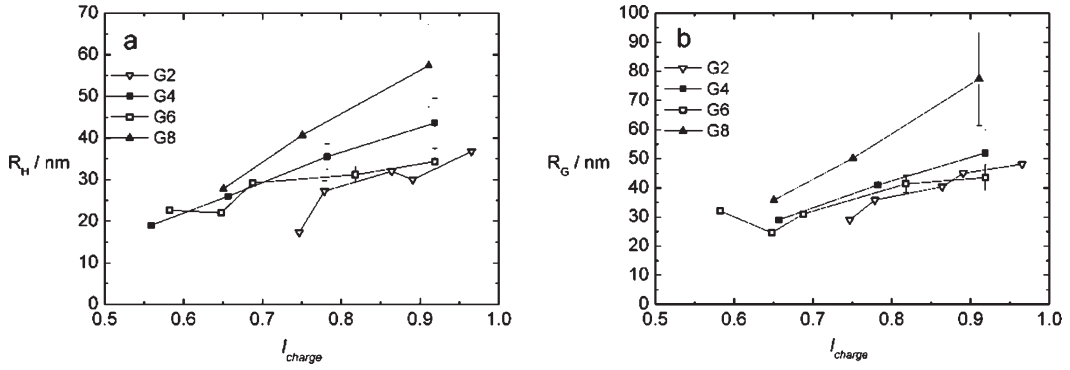

Figure 1. (a) Hydrodynamic radii and (b) radii of gyration of dendrimer−dye assemblies of Ar26 with G2, G4, G6, and G8 PAMAM dendrimer. The polymer concentration is constant for all samples.

constant, c the sample mass concentration, and $R(\theta)$ the Rayleigh ratio, i.e., the scattering intensity of the sample corrected for solvent scattering and normalized by the absolute scattering intensity of toluene. A_2 is the second virial coefficient.

ζ-Potential. ζ-Potential measurements were conducted on a DelsaNano C Particle Analyzer (Beckmann Coultier). Usually 3 runs were used.

UV−vis Spectroscopy. Absorption spectra were recorded on a Varian Cary 5000 spectrometer using quartz cuvettes with 1 cm path length.

Isothermal Titration Calorimetry. ITC measurements were carried out with a VP-ITC microcalorimeter from Microcal Inc. (Northampton, MA). For all experiments with PAMAM dendrimers and PAH, 15 to 25 injections of 10−15 μL each were used. Control dilution experiments of the individual polyelectrolytes (polyallylamine, PAMAM dendrimer) were carried out. Dilution heats were negligible in comparison to dendrimer−dye interaction energies. The dye-dilution experiment was carried out before.[47] The timespan between subsequent injections was 300 s. Precipitation of stoichiometric complexes as described in light scattering was not a problem in ITC experiments as the concentration was lower than for light scattering. In addition, the loading ratio changes rapidly, so the duration of the experiment is short enough to prevent the formation of macroscopic precipitates which guarantees exact data. All experiments were conducted at 25 °C. Formic acid/formiate was used as the buffer system with c(buffer) = 15 mmol L^{-1}. Data analysis was performed using a one-site model as implemented in MicroCal ITC data analysis software for Origin 7.0.[61]

RESULTS AND DISCUSSION

In this project, we investigate the influence of polyelectrolyte structure on the assembly properties. All investigated polyelectrolytes carry amino groups that can be deprotonated at high pH values. For a sample description, we previously introduced the loading ratio l, being the chemical ratio of the dye sulfonate groups to the primary amino groups

$$l = \frac{c(-SO_3^-)}{c(-NH_2)} \quad (3)$$

All samples in this study have a final pH of pH = 3.5, where all polymers are fully protonated,[47,62] and the loading ratio can be converted into the charge ratio representing the molar ratio of the actual charges (l_{charge})

$$l_{charge} = \frac{c(-SO_3^-)}{c(-NR_3^+)} \quad (4)$$

Therefore, charge stoichiometry for all samples is located at $l_{charge} = 1$.

To establish relations of building block architecture and assembly characteristics for the assemblies resulting from Ar26 and the different polyelectrolyte building blocks, first, the structural properties are investigated in part A. In part B, thermodynamics of the assembly formation are investigated, and in part C, a model for the dependency of the assembly characteristics on the polyelectrolyte building block is proposed.

A. Structural Characterization of Nanoparticles from Different Polyelectrolytes. Figure 1 depicts dynamic and static light-scattering results for assemblies of Ar26 and different generations of the PAMAM dendrimer (G2, G4, G6, and G8) in dependence on the charge ratio. A previous study elucidated that the dye Ar 26 (size < 1 nm) and G4 PAMAM dendrimer (radius $R \approx 2.3$ nm) can form stable assemblies with hydrodynamic radii between $R_H = 20$ nm for moderate G4 dendrimer excess ($l_{charge} = 0.55$) and $R_H = 43$ nm for low excess of G4 dendrimer ($l_{charge} = 0.95$). These radii were determined from a large set of samples as presented in ref 50 and are further confirmed by samples prepared within the present study. Samples with dendrimer excess are stable and do not change their size after the initial measurement about 20 min after preparation for several months. The size increase can be attributed to interconnection of the dendrimers through dye counterions. For $l_{charge} < 0.55$, individual dendrimers loaded with dye are the predominant species, whereas samples with dye excess ($l_{charge} > 1$) are less stable, i.e., start precipitating after a few weeks. In the range $0.55 \leq l_{charge} \leq 0.95$ selected in Figure 1, the hydrodynamic radius and the radius of gyration increase with increasing charge ratio for G2, G4, G6, and G8 dendrimers. Sizes range from $R_H = 18$ nm to $R_H = 37$ nm for G2, $R_H = 23$ nm to $R_H = 35$ nm for G6, and $R_H = 28$ nm to $R_H = 57$ nm for G8. Hence, all assembly sizes exceed the order of magnitude of the size of their building blocks (see Table 1) by about the factor 10. G8 shows the largest assemblies, while for the other generations the size of the building block does not show a clear correlation to the final assembly size. For the G2 dendrimer, samples with $l_{charge} < 0.7$ cannot be investigated by light scattering as some larger aggregates are present which complicate data analysis. The widths (standard deviation) of

Table 1. Polyelectrolytes Used in This Study and Electrophoretic Mobility of Ar26−Polyelectrolyte Samples

polymer	molecular mass/g mol^{-1}	radius/nm[a]	l_{charge}	μ_{el}/ (10^{-4} cm^2 (Vs)$^{-1}$)
PAMAM G0	517	0.75	-	-
PAMAM G2	3256	1.5	0.9	3.5 ± 0.23
PAMAM G4	14214	2.3	0.9	3.3 ± 0.38
PAMAM G6	58048	3.6	0.9	3.0 ± 0.77
PAMAM G8	233383	5.5	0.9	3.5 ± 0.54
polylysine	16150	≈ 5	0.75	3.9 ± 0.38
polyallylamine	17000	≈ 5	0.75	3.4 ± 0.23

[a] Values for G0−G8 from ref 59 and 63−65.

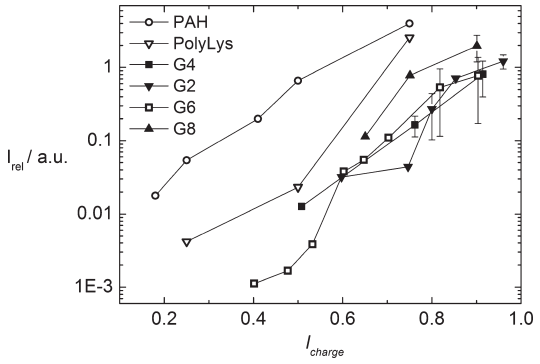

Figure 2. Relative scattering intensities for polyelectrolyte−dye assemblies of Ar26 combined with G2, G4, G6, and G8 PAMAM dendrimers and linear polyelectrolytes PAH and PolyLys.

the size distributions are usually between $0.10 \leq \sigma \leq 0.25$, which shows that the distribution of the assembly sizes is narrow and assemblies are well-defined. Radii of gyration R_G are 10%−30% larger than R_H; i.e., the characteristic ratio R_G/R_H is between 1.1 and 1.4 for G2−G8, indicating nonspherical objects. This is in accordance with the anisotropic structure of the Ar26−G4 analyzed previously by small-angle scattering.[47] For G2−G8, the scattering intensity extrapolated to zero angle depicted in Figure 2 increases by 2 to 4 orders of magnitude when the charge ratio is increased from $l_{charge} = 0.25$ to $l_{charge} = 0.90$. Thus, the dependence of the hydrodynamic radius, the radius of gyration, and the scattering intensity on the charge ratio is relatively similar for the dendrimer generations G2−G8.

In contrast, G0 does not form stable assemblies with Ar26. Samples with $0.2 < l_{charge} < 0.8$ yield hydrodynamic radii of 150 nm < R_H < 400 nm, but precipitation occurs after several hours. No systematic dependence of the charge ratio on the size of the aggregates is observed, possibly due to a more kinetically controlled process. As G0 carries 6 charges only, it can bind only 3 dye counterions electrostatically. That might be too few to enable a cooperative binding of the dye molecules to the polyelectrolyte template. Thus, a certain size difference between both building blocks is required.

Hence, the ability of the dye to interconnect dendrimers does not show an expressed dependence on the size of the latter except for dendrimers with a very low molecular mass, i.e., G0. This appears to be a general principle in such electrostatic self-assembly, as recently in a different system of anionic polystyrene sulfonate and a cationic porphyrin results indicated that the particle size does not depend substantially on the molecular mass of the polyelectrolyte as long as the molecular mass was above a certain minimum.[54] In addition, precipitation occurs once a charge ratio of unity is reached for all dendrimer generations. A charge mismatch is thus required to stabilize the nanoparticles.

Further, linear polyallylamine hydrochloride (PAH) and polylysine (PolyLys) of similar molecular masses as the G4 PAMAM dendrimer were chosen. In contrast to the dendrimer samples, for both linear polymers the onset of precipitation is found already at a charge ratio of $l_{charge} \approx 0.8$. This may be due to the slightly different binding stoichiometry, which will be discussed in section B, or the higher flexibility compared to the dendrimers, i.e., cross-linking linear polyelectrolytes into assemblies may be easier than highly charged and compact dendrimers. Figure 3 shows hydrodynamic radii R_H (a) and radii of gyration R_G (b) of PAH and PolyLys assemblies with Ar26. With increasing charge ratio, the radii increase similar to the dendrimer−dye assemblies. For PAH, sizes range from $R_H = 40$ nm at $l_{charge} = 0.18$ to $R_H =$ 200 nm at $l_{charge} = 0.75$, close to the precipitation limit, whereas PolyLys exhibits radii between $R_H = 20$ nm at $l_{charge} = 0.25$ and $R_H = 90$ nm at $l_{charge} = 0.75$. R_H and R_G for PAH show a higher variation as compared to dendrimer−dye assemblies, which may be due to a stronger kinetic barrier against rearrangements of the structure. The reported radii are final values as described for the dendrimer samples, meaning that the values for stable samples do not change for at least a few months. For both linear polyelectrolytes, the assembly size distributions were narrow with $0.1 \leq \sigma \leq 0.25$. R_G/R_H is between 1.1 and 1.4 for PolyLys in difference to PAH, where the ratio varies between 0.8 and 1.1. Thus, Ar26−PolyLys assemblies behave similarly compared to dendrimer−dye assemblies, whereas Ar26−PAH assemblies show a lower R_G/R_H ratio indicating different particle geometry. For Ar26−PAH assemblies, hydrodynamic radii and radii of gyration are larger than for Ar26−PolyLys assemblies. This may be due to the lower distance between charged amino groups. Charge distance is an important factor that can influence the stacking geometry and interaction of the dye molecules which again determines the ability of the dye molecules to interconnect the dendrimer molecules. In a system consisting of linear ionenes and pyrene tetrasulfonic acid, the charge distance was shown to influence the aggregate size significantly.[53] In addition, the PAH backbone does not contain hydrophilic moieties in difference to PolyLys, which may be a further reason for the larger sizes found for PAH because the hydrophobic backbone of PAH is expected to have a higher tendency to aggregate in water once the charged groups are ion-paired. In terms of size, PolyLys−dye assemblies are similar compared to the dendrimer−dye assemblies, which likely is due to the similar chemistry.

Electrophoretic mobilities are a useful tool to understand stabilities of electrostatically stabilized particles by providing a measure of the effective particle charge. Previous studies have shown that the source of stability for similar assemblies is charge.[50] Therefore, we herein carried out mobility measurements for polyelectrolyte−dye samples with charge ratios close to the precipitation limit for each polyelectrolyte−dye combination. Table 1 shows that all values range between $\mu_{el} = +3.0 \times 10^{-4}$ to $+3.9 \times 10^{-4}$ cm^2(Vs)$^{-1}$, which elucidates that the assemblies are stabilized by positive charge provided by excess polycation. More importantly, there are no large differences in the mobilities of the various species. This indicates that the final size, i.e., the cease of aggregate growth, is determined by charge accumulation. Positive charge accumulates in the polyelectrolyte−dye particles,

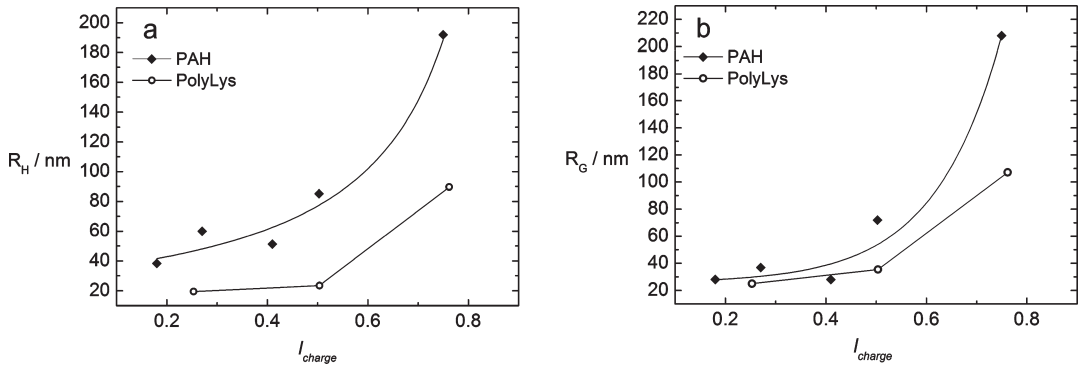

Figure 3. (a) Hydrodynamic radii R_H and (b) radii of gyration R_G of Ar26−PAH and Ar26−PolyLys assemblies.

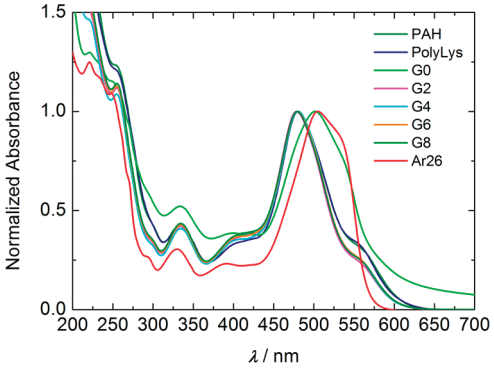

Figure 4. UV−vis spectra of Ar26−polyelectrolyte assemblies with l_{charge} = 0.75. All spectra are normalized to their absorption maximum.

as a certain excess of positively charged polyelectrolyte is present, providing electrostatic stabilization to the structure.

In conclusion of this section, the very small building block G0 dendrimer, which has a size in the range of the dye building block Ar26, does not yield stable assemblies. Hence, a certain minimum size and number of charges on the template are required for the formation of defined assemblies, possibly because only then cooperative binding occurs. G2−G8 dendrimers yield stable assemblies up to $l_{charge} \approx 0.95$ with comparable size in the range of about R_H = 15 nm to R_H = 50 nm depending on loading ratio, whereas linear polyelectrolytes yield larger assemblies up to R_H > 100 nm and precipitation occurs already at l_{charge} = 0.8. The electrophoretic mobility turned out to be similar for all polyelectrolyte species, suggesting that charge density is a crucial factor in controlling assembly size.

B. Influence of Polymer Structure on Thermodynamics of Assembly Formation. In this section, we analyze the binding of dyes to polyelectrolytes by UV−vis spectroscopy and isothermal titration calorimetry (ITC). Figure 4 shows normalized UV−vis spectra of an Ar26 solution and of samples of Ar26 with all polyelectrolytes investigated. Spectra were normalized to the absorption maximum in the wavelength range between λ = 400 nm and λ = 550 nm to focus on the spectral shape, i.e., the band splitting and spectral shifts rather than the absolute values for the extinction coefficients, as these parameters yield information on the possible arrangement of the chromophores.

It is evident that the maximum at λ = 505 nm for pure Ar26 dye shifts to $\lambda \approx (480 \pm 1)$ nm for all polyelectrolytes except for the G0 dendrimer. Figure 4 also elucidates that there is a shoulder in the spectrum corresponding to a red-shifted J-band at a wavelength of approximately $\lambda \approx 570$ nm, which is higher for the linear polyelectrolytes than for G2−G8 dendrimers having almost identical spectra. Usually, characteristic shifts occur once increments of polyelectrolyte are added to a dye solution, as the dye molecules mutually interact on the polyelectrolyte backbone and often bind cooperatively to the polyelectrolyte.[36−39] In addition to the shift of the main band absorption maximum, the spectral shape is an important factor. Typically, a band splitting and hyper- or hypsochromic effects evolve once the dye molecules interact. According to exciton theory, the chromophore dipole moments align in a specific way. Blue-shifted absorption maxima are attributed to face-to-face or H-aggregation and red-shifted maxima to head-to-tail or J-aggregation in exciton theory.[66,67] When band splitting is observed, a possible model for the arrangement is a columnar dye stack with a helical twist.[47,68] The twist angle β in a simple dimer model is proportional to the ratio between the red- and the blue-shifted absorption band, and in addition, this model allows us to estimate the chromophore distance d as we presented earlier for Ar26 and G4.[47] The twist angle β as given in ref 68 is calculated by

$$\beta = 2 \arctan\left(\sqrt{\frac{f_J}{f_H}}\right) \tag{5}$$

and the chromophore distance d by

$$d = \sqrt[3]{\frac{2.14 \times 10^7 \frac{\text{nm}^3}{\text{cm}^2} \cos(\beta)}{\nu_{mon} \Delta\nu}} \tag{6}$$

f_J and f_H are the oscillatory strength of the H- and the J-bands, whereas ν_{mon} is the wavenumber at which the absorption maximum of the monomeric dye is located and $\Delta\nu$ the splitting of the H- and the J-band maxima. As the shape of the main blue-shifted H-band with the maximum at λ = 480 nm is very similar for all spectra, the increase of the red-shifted band in the case of linear polymers corresponds to a higher twist-angle and a lower chromophore distance. More precisely, Table 2 shows that for the linear polymers the twist angle increases from 30° to 34° whereas the interchromophore distance decreases from d = 0.73 nm to d = 0.71 nm. Both twist-angle and chromophore distance are determined by two interactions, i.e., charge repulsion of the negatively charged sulfonate groups and attractive overlap

Table 2. Twist Angles and Chromophore Distances Calculated from Exciton Theory

polymer	β	d/nm
G4	30°	0.73
G6	30°	0.73
PAH	34°	0.71
PolyLys	34°	0.71

of the π-electron systems, which both counterplay. Results may be understood as there are less geometrical constraints for the linear polymers in comparison to dendritic molecules as for PAMAM dendrimers. Thus, linear polymers can adapt their conformation to enable the dye molecules to adapt the most favorable stacking geometry.

Overall, no strong influence of the polyelectrolyte building block on the spectral shape is observed. A possible explanation is that the dendrimer size does not influence the microenvironment of the dyes, determining the mode of stacking as long as a certain minimum size is exceeded, whereas a different polyelectrolyte architecture as in the case of linear PAH and PolyLys can change the chromophore arrangement slightly. However, the dye is still the dominating factor as long as a template with sufficiently small charge spacing is provided. The fact that PAH and PolyLys yield very similar UV−vis spectra is interesting, as the structural characterization showed that PAH yields significantly larger structures. Likely, the flexibility of the backbone is decisive for the microenvironment of the dye determining stacking, as long as the charges are not too far apart, whereas the chemistry of the backbone has a less expressed influence on the microenvironment but rather determines the overall particle size by providing additional hydrophobic domains favoring surface minimization and thus larger aggregates.

G0 shows a different spectrum than the other polyelectrolytes. The absorption at $\lambda = 700$ nm is not due to electronic absorption but rather to scattering of the large aggregates causing turbidity. If the Ar26−G0 sample is fractionated by centrifugation, the normalized spectrum of the supernatant is identical to the pure dye spectrum, clearly indicating that a certain amount of dye does not bind to the G0 molecule. Quantitative measurements after removal of the undefined large particles show that up to 10% of the dye molecules are not bound to the cationic dendrimer for $0.1 < l_{charge} < 0.8$. The presence of free dye molecules is in agreement with the results from section A and earlier studies where ethylamine as the monovalent counterion was shown not to form assemblies with Ar26.[47] This demonstrates that a certain minimum size of the polyelectrolyte template and thus a minimum size discrepancy between both building blocks is needed for quantitative dye binding. The fact that very large and undefined particles still form may be due to the almost point-like structure of the G0 dendrimer in contrast to higher dendrimer generations, where the dendritic structure may contribute significantly to the formation of ordered structures. This is in analogy to calculations by Pincus, who reported that the absence of geometric constraints can lead to infinite aggregate growth.[69] Likely, a certain minimum-sized template is required for cooperative and quantitative dye binding, leading to defined assemblies.

ITC gives insight into thermodynamic parameters of the polyelectrolyte−dye assemblies, whereby association enthalpies and equilibrium constants as well as stoichiometries can be determined directly allowing for calculation of the free energy and the entropy of the process. G2 and G6 dendrimers and linear PAH have been chosen for a detailed investigation of the binding thermodynamics. In Figure 5, all raw heat traces (top) and integrated heats per polyelectrolyte molecule (bottom) are depicted. For G2 and G6, the ratio between dendrimer molecules and dye molecules is given as the molar mass is well-defined, whereas in the case of the linear PAH this ratio was calculated from the amino group content per PAH mass to ensure accuracy of the stoichiometry values. All ITC titration curves in Figure 5 show negative reaction heats; i.e., the dye binding to the polyelectrolyte is an exothermic process as observed previously for the PAMAM G4 dendrimer.[47] Table 3 shows that the number of dyes binding to one polyelectrolyte molecule N corresponds to the number of charges divided by two; e.g., $N = 16$ dye molecules with each two charged sulfonate groups bind to one G2, $N = 62$ dyes to G4, and $N = 272$ dyes to one G6 molecule corresponding to a charge ratio for saturation of $l_{charge} = 1.07$ for G2, $l_{charge} = 0.98$ for G4, and $l_{charge} = 1.07$ for G6. This demonstrates that each amino group ion-pairs with approximately one sulfonate group.

For linear PAH, a slightly higher amount of dye molecules can bind per macroion ($l_{charge} = 1.11$), which may be due to the smaller spacing of charges. Overall, the binding stoichiometry is in the range for dyes binding to oppositely charged polyelectrolytes found in the literature, mostly spectroscopically. For example, in the original experiment by Schwarz, the binding stoichiometry of monovalent proflavine hydrochloride to linear polyglutamic acid was $l_{charge} = 1.1$.[70] In variance, for the binding of monovalent toluidine blue to polyvinylsulfonate the dye binds in excess with $l_{charge} = 1.5$,[71,72] whereas for the binding of aromatic azo dyes to ionenes, the ratio can be polyelectrolyte excess as reported for trivalent Acid Red 18 ($l_{charge} = 0.83$) or stoichiometric as for the divalent Acid Red 44 ($l_{charge} = 1$).[73] For the binding of methylene blue to colloid hydrogel particles $l_{charge} = 0.9$ to 1.2 is found.[74] Thus, a variety of binding stoichiometries are possible, depending on structure and valency of the dye and structure and chemistry of the polyelectrolyte. As evident from Table 3a, the enthalpy for the dye binding is in the same range for G2, G4, and G6 dendrimers, while G2 exhibits the lowest enthalpy ($\Delta H = -41$ kJ mol^{-1} for G2 compared to $\Delta H = -46.8$ kJ mol^{-1} for G6 and $\Delta H = -49$ kJ mol^{-1} for G4). Linear PAH yields a lower binding enthalpy ($\Delta H = -34.6$ kJ mol^{-1}), possibly due to the fact that overstoichiometric binding of Ar26 causes stronger repulsion between the dye molecules due to the closer proximity of the negative charges induced by the much smaller charge spacing. Earlier, we showed that for Ar26 a contribution of around $\Delta H = -30$ kJ mol^{-1} dye originates from dye−dye stacking, whereas electrostatic interactions account for the rest of the exothermic enthalpy.[47] Equilibrium constants can be calculated from eq 7 as the dendrimer molecules always become fully saturated with dye molecules on their injection into the titration cell. Until the point where all dye molecules are bound to dendrimer molecules, there always is an equilibrium between free and bound dye. The equilibrium condition is also confirmed by the fact that if the experiment is done vice versa, i.e., the dye is injected into the dendrimer, results are the same.[47]

$$\Delta G = -RT \ln(K) \tag{7}$$

All equilibrium constants are in the range of $K \approx 10^7$ L mol^{-1}, which is very high. For the dendrimers, the binding process is entropically disfavored, which is evident from the free enthalpy being less negative than the reaction enthalpy, whereas linear

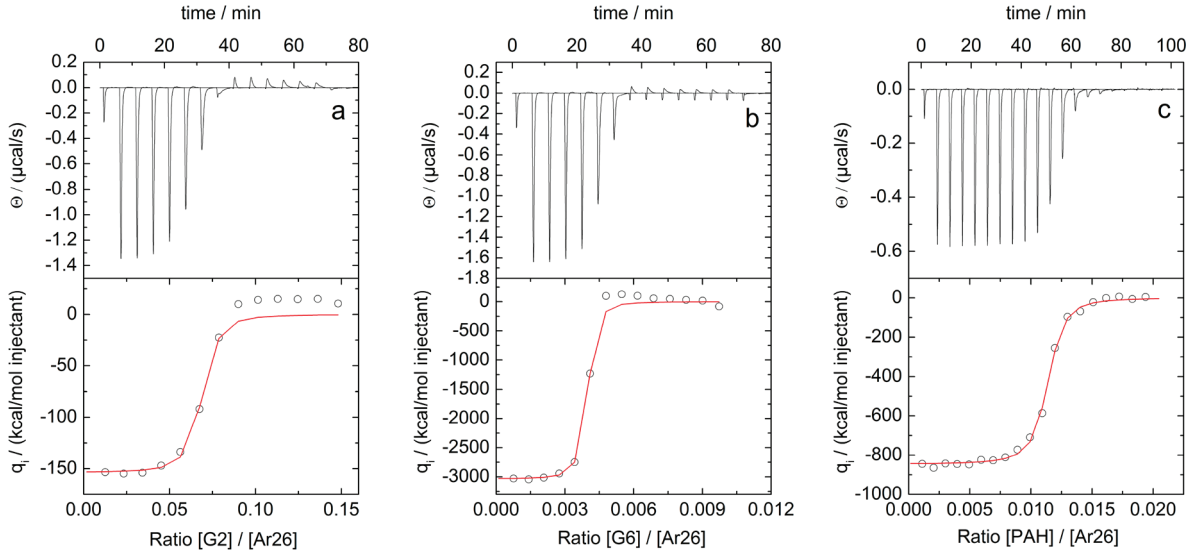

Figure 5. ITC titrations of Ar26 (titrant, cell, [Ar26] = 18.0 μmol L^{-1}): (a) with G2 PAMAM dendrimer, [G2] = 23.3 μmol L^{-1}; (b) G6 PAMAM dendrimer, [G6] = 1.42 μmol L^{-1}; and (c) linear PAH, [PAH] = 1.81 μmol L^{-1} (titrators, syringe). Reaction heats (top) and reaction enthalpies per mole of injectant (bottom, raw heat divided by the molar amount of injectant per injection). Red line corresponds to the one-site model fit.

Table 3. ITC-Data for Polyelectrolyte−Ar26 Dye Association Per (a) Dye Molecule and (b) Polyelectrolyte Molecule

(a)

polyelectrolyte	charges (pH = 3.5)	ΔH per dye/kJ mol^{-1}	N dye /$(mol\ PE)^{-1}$	K/L mol^{-1}	$T\Delta S$/kJ $(mol\ dye)^{-1}$	ΔG/kJ $(mol\ dye)^{-1}$
G2	30	−41.11 ± 1.43	16 ± 3	(1.2 ± 0.7) × 10^7	−0.74 ± 0.58	−40.37 ± 2.10
G4	126	−48.96 ± 0.76	62 ± 3	(5.0 ± 1.5) × 10^7	−5.00 ± 2.94	−43.96 ± 0.94
G6	510	−46.80 ± 0.42	272 ± 5	(2.2 ± 0.5) × 10^7	−5.54 ± 3.43	−41.36 ± 1.43
PAH	∼184	−34.63 ± 0.24	102 ± 3	(1.6 ± 0.3) × 10^7	6.50 ± 3.67	−41.13 ± 1.60

(b)

polyelectrolyte	charges (pH = 3.5)	ΔH per PE/kJ mol^{-1}	l_{charge}	$T\Delta S$/kJ $(mol\ PE)^{-1}$	ΔG/kJ $(mol\ PE)^{-1}$
G2	30	−643 ± 22	1.07	−13 ± 1	−630 ± 33
G4	126	−3013 ± 47	0.98	−308 ± 181	−2705 ± 60
G6	510	−12720 ± 114	1.07	−1471 ± 911	−11249 ± 85
PAH	∼184	−3532 ± 50	1.11	−663 ± 374	−4195 ± 96

PAH has a positive entropic contribution. Further, it is noticeable that the free energy per dye is similar for all dendrimer generations and for PAH.

As evident from Figure 5, the one-site model describes binding isotherms well up to saturation, but the part of the curve after complete binding ($1/l_{charge} > 1$) is only well fitted for the linear PAH. For the dendrimers, an endothermic reaction heat starts to evolve above saturation. Figure 6a features the endothermic heat per dendrimer molecule for injections after saturation, which is largest for G6 and decreases toward G2. If the heat is normalized to the amount of charges, the opposite trend is observed with G2 showing ΔH = +2 kJ mol^{-1} and G6 between +0.4 kJ mol^{-1} < ΔH < +1 kJ mol^{-1} (Figure 6b).

To understand the reason for this behavior, it is important to note that the major dendrimer−dye interaction energy for the dye binding process arises from mutual interaction of the dye molecules, which is strongest when the dye molecules are in spatial proximity to each other, i.e., at a stoichiometric ratio of $l_{charge} \approx 1$. If an excess of dendrimer is added to a sample of dye-rich assemblies, the interconnection between the dendrimers is disrupted as observed previously by light scattering.[46] The dendrimer-bound dye molecules become distributed between the total amount of dendrimers present in solution, which leads to a decrease in interaction energy. Therefore, the addition of excess dendrimer is endothermic due to a breakup of dye stacks. The difference between G2, G4, and G6 dendrimers and linear PAH in the second part of the binding isotherm will be further discussed in part C.

C. Model Development. Differences in assembly formation of the polyelectrolytes raise the question how structural results correlate with thermodynamic parameters. First, it is of interest why the structure formation behavior is very similar for all dendrimer generations except for G0 but different with linear polyelectrolytes. In addition, it is desirable to clarify why the ITC titrations yield similar results for the dye binding to the dendrimer in the range for dye excess, whereas differences are

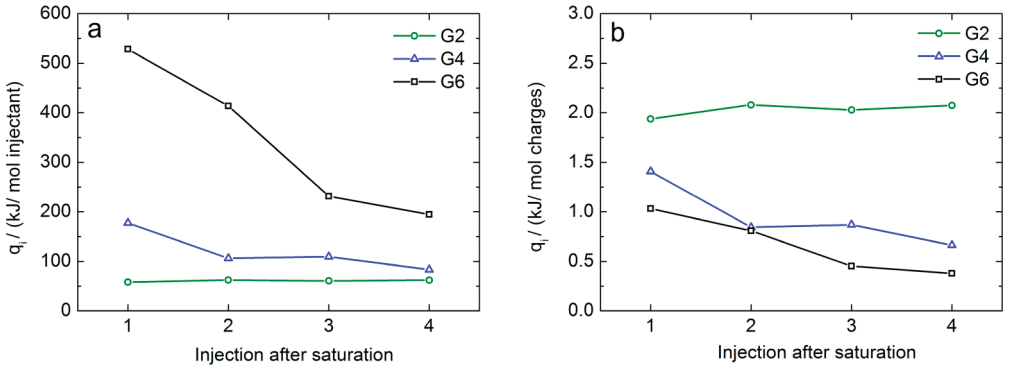

Figure 6. Enlargement of the endothermic area for G2, G4, and G6 dendrimers.

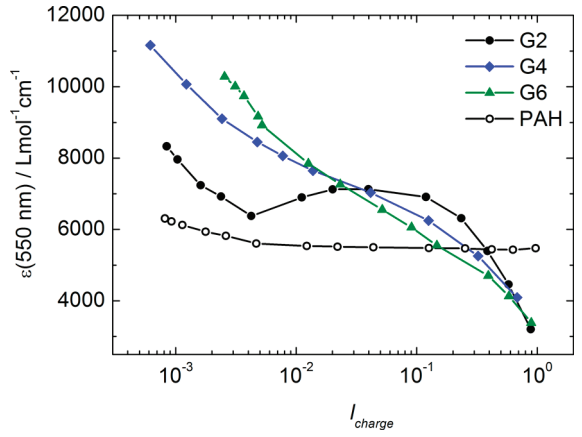

Figure 7. Extinction coefficient at λ = 550 nm for different dendrimer−dye ratios.

Scheme 2. Model Describing the Differences for Small and Large Dendrimer Generations and Their Binding Behavior When Combined with Ar26 (Red Bars)[75]

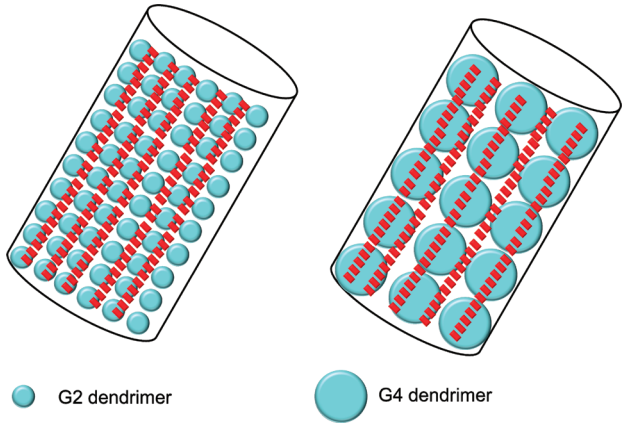

observed for dendrimer excess. For this purpose, it is feasible to monitor the dye−dye interactions by UV−vis spectroscopy. Samples with a slight excess of polyelectrolyte (l_{charge} = 0.75) were prepared, where large assemblies incorporating a high number of polyelectrolyte molecules interconnected by dye molecules are present. As evident from light scattering, further addition of polyelectrolyte caused at least in the dendrimer case the assemblies to be disrupted. This process must be accompanied by changes in dye−dye interactions. Figure 7 shows that the extinction coefficient of Ar26−dendrimer samples increases from ε_{550} = 3000 L mol^{-1}cm^{-1}, as typical for mutually interacting dye molecules, toward values found for the monomer (ε_{550} = 12500 L mol^{-1}cm^{-1}) if the charge ratio is changed gradually from l_{charge} = 0.75 to $l_{charge} \approx$ 0.001. This corresponds to a breakup of columnar dye stacks by redistribution of the dye molecules. In Scheme 2, a model of G2 and G4 assemblies with Ar26 is depicted. As G4 molecules are larger than G2, more dye molecules are bound to one individual dendrimer molecule. To form particles of the same size, columnar dye stacks therefore have to interconnect many more dendrimer molecules for lower generation dendrimers than for higher generations, and thus much more "junction points" exist where two dendrimers are interconnected.

This is evident from Figure 7, as the shape of the plot for the G2 dendrimer shows an area with a high slope when l_{charge} is decreased from l_{charge} = 0.75 to l_{charge} = 0.1. Then, a subsequent plateau region and a further increase of the extinction coefficient follow. This indicates a two-step process, where the first process at low dendrimer excess may correspond to the disruption of dye stacks interconnecting different dendrimer molecules, whereas the second process may be gradual further breakup of dye stacks located at individual dendrimers finally leading to further dispersion of the dye molecules among the added dendrimer molecules. Therefore, this initial slope is highest for the G2 dendrimer, as most junction points have to be disrupted for G2, whereas G4 and G6 show lower initial slopes due to the smaller number of dendrimer molecules interconnected in the assemblies.

The findings that the extent of breakup of dye stacks depends on the generation is in agreement with ITC-data, as G2 shows a larger endothermic heat when excess dendrimer is added as compared to G4 and G6. Thus, the endothermic part of the ITC binding isotherm on addition of excess dendrimer should be analyzed further in this context. Figure 8 shows the normalized average relative heat release per dendrimer charge for the part of the ITC titration curve where dendrimer is added in excess. This endothermic heat should be proportional to the number of dye−dye interactions cleaved by addition of excess dendrimer, which should in turn be proportional to the number of junction points. According to Scheme 2, the number of junction points may be calculated by the ratio of the building block radii, if only one dimension is considered.[76] For example, the ratio of the radii of G2 and G6 dendrimers is R_{G2}/R_{G6} = 2.0/4.1 = 0.49. Thus, dye stacks of the same length span more than twice the amount of dendrimer molecules for G2 as compared to G6, and about twice

dx.doi.org/10.1021/jp204368t |J. Phys. Chem. B 2011, 115, 9710–9719

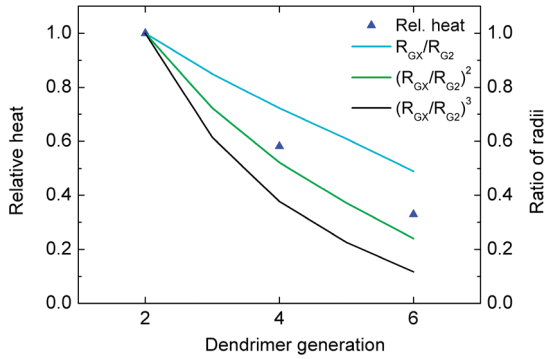

Figure 8. Correlation between building block dimensions and relative heat for overstoichiometric dendrimer addition.

the amount of junction points where dye stacks interconnect two dendrimer molecules exist. This ratio of building block radii would be expected to describe the relative heats, if rods of interconnected dendrimers comparable to a string of beads were cleaved at the junction points. In this scenario, the amount of dye stacks cleaved and thus the endothermic heat would be proportional to the relative diameter of the dendrimers. If however stacks are not all parallel to each other but may be aligned in two or three dimensions in space, the endothermic heat should be proportional to the second or third power of the ratio between the building block sizes, e.g., for G2 and G6 dendrimer in three-dimensional space: $(R_{G2}/R_{G6})^3 = 0.12$. Figure 8 depicts the heat release relative to the G2 dendrimer calculated from Figure 6b and the linear, quadratic, and cubic ratio of the building block sizes discussed above. Figure 8 shows that the experimental endothermic heat is between the values expected for one-dimensional and two-dimensional dye stack arrangement. This is reasonable as the dendrimer−dye assemblies were shown to be anisotropic.[47] The qualitative trend is represented by the proposed model. This means that the heat uptake likely is proportional to the number of junction points between dendrimers, i.e., the amount of dye−dye interactions cleaved in this process which seems to hold on at least a semiquantitative basis.

A significantly different behavior is found for linear PAH. As seen in Figure 7, the extinction coefficient is constant when excess PAH is added up to $l_{charge} = 0.01$. Hence, no decrease of dye−dye interaction happens. Most likely, PAH−dye aggregates are kinetically fixed; i.e., once an aggregate is formed, excess PAH molecules do not cause dye molecules to rearrange. Therefore, as evident from ITC, no heat uptake occurs. The reason for this may be that the flexible linear PAH molecules form a more "hairy" layer around the aggregate providing steric shielding against other PAH molecules in addition to the electrostatic repulsion. Further, the dye-binding process is entropically favored for PAH as opposed to the dendrimers. Since the breakup of dye stacks is endothermic, this process must be driven by entropy which cannot be the case for PAH. Another proof for the kinetic fixation of the aggregates is the fact that at $l_{charge} = 0.18$ particles are still formed for PAH, whereas for dendrimers only individual molecules loaded with dye form. Therefore, UV−vis and ITC correlate with the dissolution of dye-interconnected dendrimer assemblies on addition of excess dendrimer seen in light scattering.

CONCLUSION

In conclusion, we demonstrated that electrostatic self-assembly of various polyelectrolytes and dye counterions is a versatile route to supramolecular nanoparticles in solution. The concept is viable for a variety of polyelectrolyte building blocks with different sizes, geometries, and chemical compositions. The size of the polyelectrolyte building blocks turned out not to influence the assembly formation substantially as long as it was significantly larger than the dye building block, but expressed differences in assembly size and stability could be found between dendritic and linear polyelectrolytes. Assemblies were found to be stable due to electrostatic repulsion provided by excess polycation. Thermodynamic measurements combined with UV−vis spectroscopy showed that the stacking of the dye molecules is crucial for the interconnection of the dendrimer building blocks into larger assemblies and allowed us to connect the breakup energy for dye stacks to the transition from highly interconnected to individual dye-loaded dendrimers. A simple semiquantitative model based on the size of the building blocks connects the structural transition with thermodynamic parameters.

ASSOCIATED CONTENT

Supporting Information. DLS and HPLC data for the polyelectrolyte building block G4 PAMAM dendrimer. This material is available free of charge via the Internet at http://pubs.acs.org.

AUTHOR INFORMATION

Corresponding Author

*Fax: 49-9131- 85 28307. E-mail: franziska.groehn@chemie.uni-erlangen.de.

ACKNOWLEDGMENT

Financial support of Deutsche Forschungsgemeinschaft, Verband der Chemischen Industrie (VCI), and the Interdisciplinary Center for Molecular Materials (ICMM, University Erlangen-Nürnberg) is gratefully acknowledged. We are thankful to Prof. Helmut Ritter, University Düsseldorf, for letting us perform ITC measurements in his laboratory.

REFERENCES

(1) Ringsdorf, H.; Schlarb, B.; Venzmer, J. *Angew. Chem., Int. Ed.* **1988**, *27*, 113–158.
(2) Wu, C.; Gao, J. *Macromolecules* **2000**, *33*, 645–646.
(3) Antonietti, M.; Förster, S. *Adv. Mater.* **2003**, *15*, 1323–1333.
(4) Percec, V.; Dulcey, A. E.; Balagurusamy, V. S. K.; Miura, Y.; Smidrkal, J. *Nature* **2004**, *430*, 764–768.
(5) Laschewsky, A.; Mertoglu, M.; Kubowicz, S.; Thünemann, A. F. *Macromolecules* **2006**, *39*, 9337–9345.
(6) Lee, E.; Kim, J. K.; Lee, M. *Angew. Chem., Int. Ed.* **2008**, *47*, 6375–6378.
(7) Becherer, M. S.; Schade, B.; Böttcher, C.; Hirsch, A. *Chem.—Eur. J.* **2009**, *15*, 1637–1648.
(8) Koupanou, E.; Ahualli, S.; Glatter, O.; Delgado, A.; Krumeich, F.; Leontidis, E. *Langmuir* **2010**, *26*, 16909–16920.
(9) Göbl, C.; Dulle, M.; Hohlweg, W.; Grossauer, J.; Falsone, S. F.; Glatter, O.; Zangger, K. *J. Phys. Chem. B* **2010**, *114*, 4717–4724.
(10) Gröhn, F. *Soft Matter* **2010**, *6*, 4296–4302.
(11) Antonietti, M.; Maskos, M. *Macromolecules* **1996**, *29*, 4199–4205.
(12) Ober, C. K.; Wegner, G. *Adv. Mater.* **1997**, *9*, 17–31.

(13) Thünemann, A. F.; Beyermann, J. *Macromolecules* **2000**, *33*, 6878–6885.
(14) Thünemann, A. F.; Müller, M.; Dautzenberg, H.; Joanny, J. F. O.; Löwen, H. *Adv. Polym. Sci.* **2004**, *166*, 113–171.
(15) Bai, G.; Bastos, M. *J. Phys. Chem. B* **2005**, *109*, 518–525.
(16) Li, Y.; Wang, D.; Hao, Z.; Hao, J.; Han, C. C. *Chem.—Eur. J.* **2007**, *13*, 4782–4785.
(17) Xu, Y.; Bolisetty, S.; Ballauff, M.; Müller, A. H. E. *J. Am. Chem. Soc.* **2009**, *131*, 1640–1641.
(18) Gröhn, F.; Bauer, B. J.; Amis, E. J. *Macromolecules* **2001**, *34*, 6701–6707.
(19) Sinn, C. G.; Dimova, R.; Antonietti, M. *Macromolecules* **2004**, *37*, 3444–3450.
(20) Goerigk, G.; Huber, K.; Schweins, R. *J. Chem. Phys.* **2007**, *127*, 154908.
(21) Pochan, D. J.; Chen, Z. Y.; Cui, H. G.; Hales, K.; Qi, K.; Wooley, K. L. *Science* **2004**, *306*, 94–97.
(22) Berret, J.-F. *Macromolecules* **2007**, *40*, 4260–4266.
(23) Duschner, S.; Störkle, D.; Schmidt, M.; Maskos, M. *Macromolecules* **2008**, *41*, 9067–9071.
(24) Nizri, A.; Makarsky, S.; Magdassi; Talmon, Y. *Langmuir* **2009**, *25*, 1980–1985.
(25) Lemmers, M.; Sprakel, J.; Voets, I. K.; van der Gucht, J.; Cohen Stuart, M. A. *Angew. Chem., Int. Ed.* **2010**, *49*, 708–711.
(26) Förster, S.; Hermsdorf, N.; Leube, W.; Schnablegger, H.; Regenbrecht, M.; Akari, S. *J. Phys. Chem. B* **1999**, *103*, 6657–6668.
(27) Zhang, Y.; Guan, Y.; Yang, S.; Xu, J.; Han, C. C. *Adv. Mater.* **2003**, *15*, 832–834.
(28) Gröhn, F. *Macromol. Chem. Phys.* **2008**, *209*, 2295–2301.
(29) Tirumala, V. R.; Tominaga, T.; Lee, S.; Butler, P. D.; Lin, E. K.; Gong, J. P.; Wu, W. *J. Phys. Chem. B* **2008**, *112*, 8024–8031.
(30) Loizou, E.; Porcar, L.; Schexnailder, P.; Schmidt, G.; Butler, P. *Macromolecules* **2010**, *43*, 1041–1049.
(31) Jones, G.; Rahman, M. A. *J. Phys. Chem.* **1994**, *98*, 13028–13037.
(32) Petzold, G.; Schwarz, S.; Mende, M.; Jaeger, W. *J. Appl. Polym. Sci.* **2007**, *104*, 1342–1349.
(33) Zhang, Q.; Bazuin, C. G.; Barrett, C. J. *Chem. Mater.* **2008**, *20*, 29–31.
(34) Dragan, E. S.; Dinu, I. A. *J. Appl. Polym. Sci.* **2009**, *112*, 728–735.
(35) van Grondelle, R.; Novoderezhkin, V. *Biochemistry* **2001**, *40*, 15057–15068.
(36) Schwarz, G. *Eur. J. Biochem.* **1970**, *12*, 442–453.
(37) McGhee, J. D.; von Hippel, P. H. *J. Mol. Biol.* **1974**, *86*, 469–489.
(38) von Tscharner, V.; Schwarz, G. *Biophys. Struct. Mech.* **1979**, *5*, 75–90.
(39) Handel, T. M.; Cohen, H. L.; Tan, J. S. *Macromolecules* **1985**, *18*, 1200–1206.
(40) Neumann, B.; Huber, K.; Pollmann, P. *Phys. Chem. Chem. Phys.* **2000**, *2*, 3687–3695.
(41) Moreno-Villoslada, I; Jofre, M.; Miranda, V.; Gonzalez, R.; Sotelo, T.; Hess, S.; Rivas, B. L. *J. Phys. Chem. B* **2006**, *110*, 11809–11812.
(42) Moreno-Villoslada, I.; Gonzalez, F.; Rivera, L.; Hess, S.; Rivas, B. L.; Shibue, T.; Nishide, H. *J. Phys. Chem. B* **2007**, *111*, 6146–6150.
(43) Moreno-Villoslada, I.; Torres-Gallegos, C.; Araya-Hermosilla, R.; Nishide, H. *J. Phys. Chem. B* **2010**, *114*, 4151–4158.
(44) Krohne, K.; Duschner, S.; Störkle, D.; Schmidt, M.; Maskos, M. *Macromolecules* **2010**, *43*, 8645–8650.
(45) Duschner, S.; Gröhn, F.; Maskos, M. *Polymer* **2006**, *47*, 7391–7396.
(46) Willerich, I.; Gröhn, F. *Chem.—Eur. J.* **2008**, *14*, 9112–9116.
(47) Willerich, I.; Ritter, H.; Gröhn, F. *J. Phys. Chem.* **2009**, *113*, 3339–3354.
(48) Li, Y.; Yildiz, U. H.; Müllen, K.; Gröhn, F. *Biomacromolecules* **2009**, *10*, 530–540.
(49) Gröhn, F; Klein, K.; Koynov, K. *Macromol. Rapid Commun.* **2010**, *31*, 75.
(50) Willerich, I.; Li, Y.; Gröhn, F. *J. Phys. Chem. B* **2010**, *114*, 15466–15476.
(51) Willerich, I.; Gröhn, F. *Angew. Chem., Int. Ed.* **2010**, *49*, 8104–8108.
(52) Ruthard, C.; Maskos, M.; Kolb, U.; Gröhn, F. *Macromolecules* **2009**, *42*, 830–840.
(53) Yildiz, U. H.; Koynov, K.; Gröhn, F. *Macromol. Phys. Chem.* **2009**, *210*, 1678–1690.
(54) Ruthard, C.; Maskos, M.; Kolb, U.; Gröhn, F. *J. Phys. Chem. B* **2011**, *115*, 5716–5729.
(55) Willerich, I.; Schindler, T.; Ritter, H.; Gröhn, F. *Soft Matter* **2011**, *7*, 5444–5550.
(56) Willerich, I.; Gröhn, F. *Macromolecules* **2011**, *44*, 4452–4461.
(57) Ruthard, C.; Maskos, M.; Yildiz, H.; Gröhn, F. *Macromol. Rapid Commun.* **2011**, *32*, 523–527.
(58) Ruthard, C.; Schmidt, M.; Gröhn, F. *Macromol. Rapid Commun.* **2011**, *32*, 706–711.
(59) Prosa, T. J.; Bauer, B. J.; Amis, E. J. *Macromolecules* **2001**, *34*, 4897–4906.
(60) Provencher, S. W. *Comput. Phys. Commun.* **1982**, *27*, 229–242.
(61) Wiseman, T.; Williston, S.; Brandts, J. F.; Lin, L. N. *Anal. Biochem.* **1989**, *179*, 131–137.
(62) Cakara, D.; Kleimann, J.; Borkovec, M. *Macromolecules* **2003**, *36*, 4201–4207.
(63) Topp, A.; Bauer, B. J.; Tomalia, D. A.; Amis, E. J. *Macromolecules* **1999**, *32*, 7232–7237.
(64) Nisato, G.; Ivkov, R.; Amis, E. J. *Macromolecules* **2000**, *33*, 4172–4176.
(65) Lee, I.; Athey, B. D.; Wetzel, A. W.; Meixner, W.; Baker, J. R. *Macromolecules* **2002**, *35*, 4510–4520.
(66) Kasha, M.; Rawls, H. R.; El-Bayoumi, M. A. *Pure Appl. Chem.* **1965**, *11*, 371–392.
(67) Kasha, M.; El-Bayoumi, M. A.; Rhodes, J. *J. Chim. Phys. Phys.-Chim Biol.* **1961**, *58*, 916–925.
(68) Neumann, B.; Huber, K.; Pollmann, P. *Phys. Chem. Chem. Phys.* **2000**, *2*, 3687–3695.
(69) Henle, M. L.; Pincus, P. A. *Phys. Rev. E* **2005**, *71*, 060801.
(70) Schwarz, G.; Klose, S.; Balthasar, W. *Eur. J. Biochem.* **1970**, 454–460.
(71) Horn, D. *Prog. Colloid Polym. Sci.* **1978**, *65*, 251–264.
(72) Horn, D.; Heuck, C.-C. *J. Biol. Chem.* **1983**, *258*, 1665–1670.
(73) Dragan, S.; Cristea, M.; Airninei, A. *Macromol. Rapid Commun.* **1997**, *18*, 541–545.
(74) Soedjak, H. S. *Anal. Chem.* **1994**, *66*, 4514–4518.
(75) The anisotropic shape of the Ar26−G4 assembly has been proven previously by SANS (ref 47), while the G2 assembly shape is hypothetically displayed as anisotropic for comparison.
(76) Since the dye stacks also occupy volume in the assembly, 0.5 nm was added to the radii of the dendritic building blocks from Table 1. For one dimension, the number of junction points can be calculated by the ratio of the diameters of the building blocks as the number of objects in a one-dimensional array of a fixed length depends only on the relative diameter of the latter R_1/R_2. For a two-dimensional array, the number of objects in a plane of fixed area depends on the relative area of the individual objects, i.e., on $(R_1/R_2)^2$. The number of objects in a fixed volume depends on their relative volume, i.e., $(R_1/R_2)^3$.